UNVEILING EARTHQUAKE-INDUCED DEFORMATIONS: INSIGHTS FROM KAHRAMANMARAŞ SEISMIC EVENT USING AUSPOS ONLINE GPS PROCESSING SERVICE

[1], * Burhaneddin BİLGEN iD

[1] Ankara Hacı Bayram Veli University, Academy of Land Registry and Cadastre, Ankara, TÜRKİYE
[1]burhaneddin.bilgen@hbv.edu.tr

Highlights

- Height increased significantly at MAR1 station one day before the earthquake.

- Some distant IGS stations showed significant displacements.

- AUSPOS outputs can be used for geodetic deformation analysis.

*Corresponding Author: Burhaneddin BİLGEN, burhaneddin.bilgen@hbv.edu.tr

UNVEILING EARTHQUAKE-INDUCED DEFORMATIONS: INSIGHTS FROM KAHRAMANMARAŞ SEISMIC EVENT USING AUSPOS ONLINE GPS PROCESSING SERVICE

1, * Burhaneddin BİLGEN (iD)

1 *Ankara Hacı Bayram Veli University, Academy of Land Registry and Cadastre, Ankara, TÜRKİYE*
1burhaneddin.bilgen@hbv.edu.tr

ABSTRACT: Determination of crustal movement through geodetic deformation analysis methods provides a better understanding of the severity of the earthquakes. The widespread use of continuously operating GPS stations allows the deformations caused by earthquakes to be investigated with GPS data. In this study, the movements of Continuously Operating Reference Stations-Türkiye (CORS-Tr) stations affected by the Kahramanmaraş earthquakes (Mw 7.7 and Mw 7.6), which was felt in a wide area, were investigated in detail. It is aimed to detect and analyse co-seismic and absolute deformations due to the Kahramanmaraş earthquakes using AUSPOS-online GPS processing service and Iteratively Weighted Similarity Transformation (IWST). Ten stations were selected from the provinces in the earthquake impact area and their 28-day RINEX data, covering before and after the earthquake, were used. The data were processed using AUSPOS. Geodetic deformation analyses were performed using two epoch measurements of established deformation network via in-house software. In addition, the displacements of the two stations close to the epicentre during the monitoring period were revealed by 28-day GPS coordinate time series. Conclusively, it was observed that final S-transformation-derived absolute deformations and average coordinate-derived co-seismic deformations are highly consistent. The results showed that the largest absolute deformation occurred at the EKZ1 station with 4.68m, that was the closest station to the epicentre of the aftershock (Mw 7.6). The absolute deformation at station MAR1, which is the second near station to the epicentre of the aftershock, is 62.5 cm. All Cors-Tr stations were unstable according to deformation analysis results. In particular, unusual vertical movements observed one day prior to the earthquake at the MAR1 station in Kahramanmaraş may indicate potential pre-seismic deformation signals, highlighting the potential of the proposed method for earthquake-related monitoring.

Keywords: AUSPOS, Coseismic Displacement, Deformation, GPS, Kahramanmaraş Earthquake

1. INTRODUCTION

Earthquakes are comprehensive phenomena related to movements of the surface mass and interior of the Earth at various scales [1], [2]. Many tectonic earthquakes occur because of the movements of the plates that make up the crust of earth. Since the occurrence of earthquakes cannot be prevented, required measures must be taken to decrease the number of deaths and property loss.

Deformations can be defined as shape variations on the crust of earth due to plate movements, slipping of land masses, tidal events, and events in the hydrosphere and atmosphere [3]. Deformations, which were previously determined by classical terrestrial measurement methods, can be determined by satellite-based methods nowadays, depending on the developments in technology. Global Positioning System (GPS), one of the satellite-based methods, is widely used for point positioning and deformation monitoring [4], [5], [6], [7], [8], [9], [10], [11].

Since Türkiye is in the region where the Eurasian, Arabian and African plates merge, it has witnessed many earthquakes originating from East Anatolian Fault Zone (EAFZ) and North Anatolian Fault Zone (NAFZ). These two fault zones and earthquakes around the world have become the subject of many scientific studies with the widespread use of continuously operating GPS stations [6], [12], [13], [14], [15], [16], [17]. Bulbul et al. [12] investigated the impact of the February 6, 2023 Kahramanmaraş earthquakes

*Corresponding Author: Burhaneddin BİLGEN, burhaneddin.bilgen@hbv.edu.tr

on CORS-Tr stations by analysing GNSS data to assess coordinate shifts, baseline vector changes, and area variations before and after the event. The largest displacement, up to 4.67 meters, was observed at the EKZ1 station, with statistically significant changes detected across multiple stations. Ozkan et al. [13] analysed the co-seismic displacements and fault slip distributions of the Mw 7.7 and 7.6 earthquakes that struck the East Anatolian Fault Zone on February 6, 2023, using a dense GNSS network of 113 stations. Results revealed maximum displacements up to 466 cm and fault slips of 7.25 m and 9.43 m, highlighting significant left-lateral ruptures and fault interactions during the consecutive events. Li et al. [14] investigates the static and dynamic coseismic displacements from the Mw 7.8 and 7.6 earthquakes on February 6, 2023, using GNSS data from 56 static and 15 dynamic stations across Türkiye. Results revealed maximum slips of 10.7 m and 11.6 m along the Pazarcık and Çardak fault segments, respectively, and suggest that the Mw 7.8 event likely triggered the Mw 7.6 earthquake through Coulomb stress transfer. Kobayashi et al. [18] used InSAR ScanSAR data to map extensive ground displacements from the 2023 Kahramanmaraş earthquakes, revealing dominant left-lateral ruptures along the Erkenek–Pazarcık–Amanos and Çardak segments of the East Anatolian Fault. Gualandi et al. [19] analysed the co-seismic and post seismic deformations resulting from the 2009 L'Aquila earthquake (central Italy) of Mw 6.3 using GPS time series and determined that there were slips on both the fault where the main shock occurred and a different fault where two large aftershocks occurred. Wu et al. [20] investigated crustal deformations before the Mw 8.0 Wenchuan earthquake using GPS velocities from approximately seven hundred stations in western China. Determined GPS strain rates showed that extensional deformation was prevailing in the west of the fault where the earthquake occurred, and compressional deformation was prevailing in the east. Klein et al. [21] elaborately analysed the Illapel earthquake of Mw 8.3 in terms of slip distribution with InSAR and continuous GPS data. Wang et al. [22] investigated the slip distribution in four different earthquakes that occurred in Italy between 2009 and 2016 with GPS and InSAR data.

Starting point of the EAFZ is Karlıova/Bingöl in the northeast Anatolia. The EAFZ passes through southeast of Kahramanmaraş and reaches the Mediterranean Sea [23]. EAFZ is a left-lateral strike-slip fault that formed on the Anatolian plate because of the Arabian plate pushing the Eurasian plate. The Anatolian plate moves relative to the Arabian plate and slips towards the west [24], [25]. The relative movement of the plate varies between 6-10 mm/year and can cause devastating earthquakes in that region [26]. Ambraseys and Jackson [27] stated that there were three major historical earthquakes on the EAFZ (29 November 1114 Mw > 7.8, 28 March 1513 Mw > 7.4 and 2 March 1893 Mw > 7.1). The last major earthquakes on the EAFZ occurred on 6 February 2023, with epicenters in Pazarcık (Mw 7.7) and Elbistan (Mw 7.6). The depth of first (Mw 7.7) earthquake was 8.6 km, and the depth of the other earthquake was 7 km. "Türkiye Earthquake Hazard Map", which was updated and entered into force on 1 January 2019, shows the Peak Ground Acceleration (PGA). In the Türkiye Earthquake Hazard Map, the maximum acceleration value of PGA 475year in Kahramanmaraş varies between 0.2-0.6g. This shows that the earthquake risk of the area is relatively high, especially in the south-southeast section of the province along the EAFZ (Figure 1).
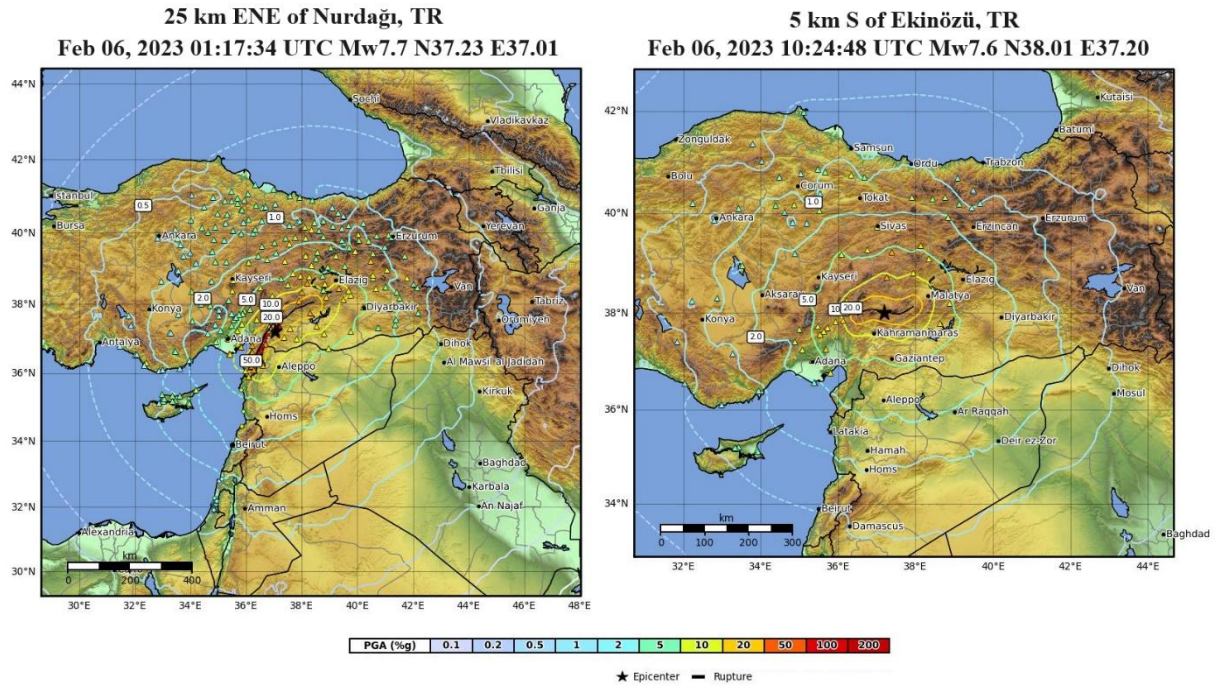
Figure 1. PGA maps for Mw7.7 and Mw7.6 Kahramanmaraş earthquakes
(https://earthquake.usgs.gov/earthquakes/eventpage/us6000jllz/shakemap/pga)

The southeast of the provincial borders is generally under the effect of the EAFZ. The EAFZ passes through the southeast of the province. Besides, the Southeastern Anatolian Fault Zone and the Ecemiş and Karataş-Yumurtalık faults in the south are important tectonic structures in the region. Çardak Fault, Pazarcık, Türkoğlu, Gölbaşı, Çelikhan-Sürgü Faults, which divide the provincial borders into two in E-W direction, are active faults in the region, and generally the main tectonic structures trend NE-SW (Figure 1).

According to AFAD [28], the Pazarcık earthquake (Mw 7.7) is in the Narlı Segment at the northern finish of the Dead Sea Fault Zone, while the Elbistan earthquake (Mw 7.6) is in the Çardak Fault, a branch separated from the EAFZ. Analysing the effects of these earthquakes on the earth's crust using GPS technology is an important research topic. Since each earthquake occurs with different dynamics, its effects may be different. In this paper, we aim to reveal these effects and, unlike many studies in the past, two-period deformation analyses were carried out with the Iteratively Weighted Similarity Transformation (IWST) method in the GPS network, which were used to determine point coordinates. Since deformation analysis is a process that uses statistics and has an intense calculation load, previous studies have ignored applying this analysis in determining absolute deformations. Another novel aspect of this study is that AUSPOS – online GPS processing service (AUSPOS) used to process GPS data for earthquake induced deformation research. In this context, the paper is one of the few researches that use AUSPOS in earthquake studies [29], [30].

This study is particularly significant as it combines AUSPOS, a widely accessible online GPS processing tool, with the IWST method to analyse earthquake-induced deformations. Unlike previous research, this approach enables a cost-effective and replicable method for identifying co-seismic and potentially pre-seismic deformation patterns, contributing a novel framework to earthquake geodesy studies.

In this study, the movements of CORS-Tr stations affected by the Kahramanmaraş earthquake sequence, which were felt in many provinces in a wide area covering the Central Anatolia, Southeastern Anatolia and the Mediterranean Regions, were elaborately investigated. Ten stations were selected from the provinces where the earthquake was felt, and their 28-day data, covering the pre- and post-earthquake periods, were processed with AUSPOS. As a result of the processing, the time series of the stations were

obtained, and their position changes compared to the pre-earthquake period were revealed. Finally, deformation analyses were performed using GPS data processing results from one day before and one day after the earthquake. Earthquake induced absolute deformations caused by the earthquake were revealed through final S-transformation method.

2. METHODOLOGY AND DATA PROCESS

Within the scope of the application, ten CORS-Tr stations (EKZ1, MAR1, ADY1, ANTE, MLY1, HAT2, ONIY, KLS1, ADN2, AKLE) located in the provinces affected by the Kahramanmaraş earthquakes that occurred on 6 February 2023, were selected (Figure 2). For clearly revealing the effect of the earthquakes, 28-day (23 January to 20 February 2023) consecutive GPS data of the stations, covering the periods before and after the earthquakes, were obtained from the CORS-Tr website. The obtained RINEX data is 24 hours duration, and its recording interval is 30 seconds.
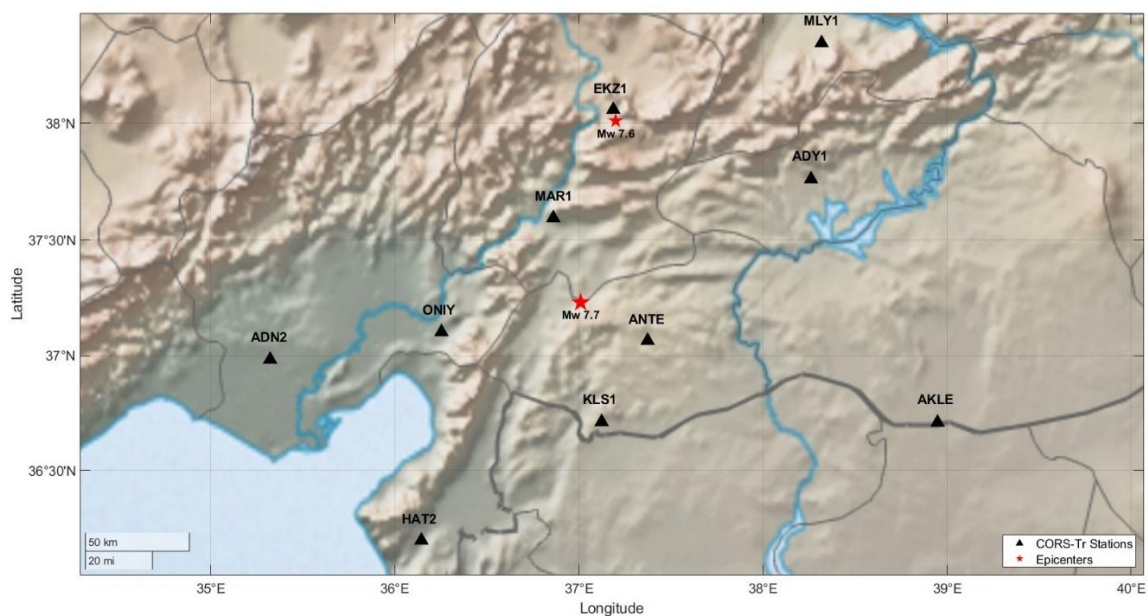
Figure 2. Epicentres of earthquakes and surrounding CORS-Tr Stations

24-hour RINEX data of ten stations were processed using AUSPOS. AUSPOS is a free online GPS data processing service presented by Geoscience Australia. It uses only GPS data in data processing and automatically decimates 1-second static datasets to a data rate of 30 seconds. It benefits both the International GNSS Service (IGS) network and IGS products. It works with GPS data gathered anywhere on the earth. Users can send dual frequency geodetic GPS RINEX data observed in 'Static' mode to the AUSPOS online processing system. A results report containing Australian Geocentric Datum 2020 (GDA2020), Australian 1994 Geocentric Datum (GDA94) and International Terrestrial Reference Frame (ITRF) coordinates will be emailed to users. (https://www.ga.gov.au/scientific-topics/positioning-navigation/geodesy/auspos). AUSPOS uses relative GPS technique in data processing and realizes the solutions with Bernese GNSS Software. Bernese is a high-precision orbit determination and geodetic parameter estimation software. For more information, see http://www.bernese.unibe.ch/. Since AUSPOS is a Bernese-based service, the result report includes the coordinates, root mean square errors and covariance matrices obtained as a result of geodetic network adjustment. Therefore, geodetic deformation analyses can also be performed using outputs of AUSPOS.

Earth orientation parameters, precise orbit files, and solution products provided by IGS and iono-free linear combination (LC) technique were used to process the data. While processing the data, automatically selected 14 nearby IGS and Asia-Pacific Reference Frame (APREF) stations were used as reference stations. Then, using these stations, an exact solution was calculated with the 'double differences' technique. The

coordinates of IGS stations are limited to 1 mm and 2 mm uncertainties horizontally and vertically, respectively. The 3D cartesian coordinates were calculated by GPS data processing with AUSPOS. The calculated GPS coordinates were converted into local geodetic coordinates (east, north, up) to independently determine the horizontal and vertical motions of the stations. Local geodetic coordinates are therewithal called topocentric coordinates. For detailed information about obtaining local geodetic coordinates, see Hoffman-Wellenhof et al. [31]. After this transformation, co-seismic displacements were obtained by taking the difference of the average CORS-Tr GPS station coordinates obtained before and after the earthquake. Equation (1) was used in the calculation of displacements.

$$d = \sqrt{\Delta n^2 + \Delta e^2 + \Delta u^2} \tag{1}$$

Where Δn, Δe, Δu represent co-seismic displacements in the direction of topocentric coordinate axes. After calculating co-seismic displacements, the coordinate differences of the stations on successive days during the 28-day monitoring period were calculated with Equation (2).

$$\begin{aligned} dn &= n_{i+1} - n_i \\ de &= e_{i+1} - e_i \\ du &= u_{i+1} - u_i \end{aligned} \tag{2}$$

Where *dn*, *de*, *du* represent daily coordinate differences, subscript *i+1* indicates the coordinates of the relevant day, and subscript *i* indicates the coordinates of the previous day. In order to analyse the change in the coordinates of the stations, time series were generated from local geodetic coordinates estimated with a horizontal accuracy of 3.0-4.0 mm and a vertical accuracy of 7.0-8.0 mm for 28 days.

After these procedures, deformation analyses were performed in the geodetic network using the 3D Cartesian GPS coordinates and their associated covariance matrices in the AUSPOS result reports thanks to an in-house software and absolute deformations caused by the earthquake were determined. IWST method was used in the deformation analyses. The IWST is a robust technique used in 3D geodetic networks for determination of deformations. The method does not require prior distinction of reference and object stations in the geodetic deformation network. Besides, the outputs indicate the actual deformation pattern and allow the characterization of the best datum as it has the least deterioration effect on the point displacements. The method can be used performing deformation analysis in GPS networks. The mathematical model of method was given in Chen et al. [32]; Gokalp and Tasci [33]; Konakoglu and Gokalp [34]. In the application of IWST, measurements of two epochs are adjusted freely. As a result of two separate free adjustment, the root mean square errors of the unit-weighted measurement (σ_1, σ_2), the adjusted coordinates of the points in the network ($\hat{x}_1$, $\hat{x}_2$), and the cofactor matrices ($Q_{\hat{x}_1}$, $Q_{\hat{x}_2}$) are calculated. To determine whether two epoch measurements have the same precision, a variance analysis based on the hypothesis $H_0: \sigma_1^2 = \sigma_2^2$ is performed;

$$\frac{\sigma_1^2}{\sigma_2^2} < F_{df_1, df_2, 1-\alpha} \tag{3}$$

If equation (3) is achieved, the variances are homogeneous. If the test is invalid, the measurements are considered to be mismatched or incorrectly weighted between the two adjustments. The displacement vector (*d*) and its cofactor matrix (Q_d) from two separate adjustment results;

$$d = \hat{x}_2 - \hat{x}_1 \qquad\qquad Q_d = Q_{\hat{x}_1} + Q_{\hat{x}_2} \tag{4}$$

The first matrix that must be calculated at the beginning of the deformation analysis is the weight matrix *P*. For the first iteration (k=1), the matrix *P* is equal to the identity matrix *I*. In the application of IWST method, the weight matrix *P* is obtained iteratively. In this case, in the second (k+1) and subsequent

successive iterations, the diagonal elements of the weight matrix;

$$P^{(k+1)}(i,i) = diagonal\{1/|d^{(k)}|\} \tag{5}$$

After these operations $d^{(k+1)}$ is calculated with the following equation:

$$d^{(k+1)} = \left\{I - G\left[G^T P^{(k+1)} G\right]^{-1} G^T P^{(k+1)}\right\}\left[d^{(k)}\right] \tag{6}$$

$$d^{(k+1)} = \left[S^{(k+1)}\right]\left[d^{(k)}\right] \tag{7}$$

Where, the dimensions of the G matrix are different for 1D, 2D and 3D networks and the datum varies depending on the defect number. G matrix for GPS networks:

$$G^T = \begin{bmatrix} 1 & 0 & 0 & 1 & 0 & 0 & 0 & 1 & 0 & 0 \\ 0 & 1 & 0 & 0 & 1 & 0 & 0 & 0 & 1 & 0 \\ 0 & 0 & 1 & 0 & 0 & 1 & 0 & 0 & 0 & 1 \end{bmatrix} \tag{8}$$

The iterative process continues until the absolute differences between successive transformed displacements (d) are less than the tolerance value δ (0.0001 m).

$$\left|d^{(k+1)} - d^{(k)}\right| < \delta \tag{9}$$

For the last iteration (k+1), the cofactor matrix:

$$Q_d^{(k+1)} = S^{(k+1)} Q_d \left|S^{(k+1)}\right|^T \tag{10}$$

To identify possible unstable points in the network:

$$c_i = \frac{d_i^2}{q_{d_i}\hat{\sigma}_0^2} \tag{11}$$

Where d_i i[th] displacement component, q_{d_i} cofactor value of the ith displacement component, $\hat{\sigma}_0^2$ is the common variance factor from equation (13);

$$c_i \leq F_{1,df,1-\alpha} \tag{12}$$

If equation (12) is achieved, the displacement of the point is not significant. Otherwise, it can be considered that the displacement of the point is significant. Where, α is the probability of error and df is the sum of the degrees of freedom for the 1st and 2nd epochs. Common variance factor;

$$\hat{\sigma}_0^2 = \frac{df_1\sigma_1^2 + df_2\sigma_2^2}{df_1 + df_2} \tag{13}$$

Where σ_1^2 and σ_2^2 are the variances for the 1st and 2nd epochs, df_1 and df_2 are the degrees of freedom for the 1st and 2nd epochs.

After these procedures, the absolute deformations at the stations were determined by the final S-transformation performed on the geodetic network created to determine the point coordinates. Elaborative information about S-transformation can be found in Doganalp et al. [35]; Yigit and Inal [36]; Even-Tzur [37]; Velsink [38] and Aydin [39]. In the final S-transformation, the elements of the P weight matrix are taken as 1 for stable reference points and 0 for the others. In the final iteration, the displacement vector and the final cofactor matrix;

$$d^{(F)} = [S^{(F)}][d^{(k+1)}] \tag{14}$$
$$Q_d^{(F)} = S^F Q_d [S^{(F)}]^T \tag{15}$$

Where, based on the application of the statistical test in equation (16), $S^{(F)} = I - G[G^T P^{(F)} G]^{-1} G^T P^{(F)}$, and $P^{(F)} = 1$ for fixed points and 0 for others.

Once the cofactor matrix and displacement vector of each point are calculated, the stability information for each point can be determined by a single point test. The displacement values and its cofactor matrix are compared to a critical value. Assuming that point i is tested, the test value;

$$T_i = \frac{d_i^T Q_{d_i}^{-1} d_i}{m \hat{\sigma}_0^2} \leq F_{m,df,1-\alpha} \tag{16}$$

Where, d_i is the displacement vector of point i, Q_{d_i} is the cofactor matrix of the displacement vector of point i, m is the dimension of the confidence level (3 for GPS networks), df is the sum of the degrees of freedoms for adjustments of the epoch measurements used in the analysis, α is the probability of error (usually 0.05), $\hat{\sigma}_0^2$ is the common variance factor. If the test in equation (16) is achieved, point i has not undergone deformation at the $1 - \alpha$ confidence level. On the other hand, if the test fails, it is decided that point i has undergone deformation.

3. RESULTS AND DISCUSSION

Co-seismic displacements caused by the 6 February 2023, Kahramanmaraş/Türkiye earthquake sequence (Mw 7.7 and Mw 7.6) were estimated using the differential GPS technique. RINEX data from ten CORS-Tr stations close to the earthquake epicentres were used for this goal (Figure 2). The 28-day data of each station in Figure 2 was processed using AUSPOS. The obtained Cartesian coordinates were converted into local geodetic coordinates in order to clearly see the vertical and horizontal motions. Co-seismic displacement was calculated by subtracting the average of the 13-day coordinates before the earthquake from the average of the 13-day coordinates after the earthquakes. The displacement vector was calculated using Equation (1) and is presented in Table 1.

Table 1. Calculated co-seismic displacements

Station	North (cm)	East (cm)	Up (cm)	Displacement vector (cm)
ADN2	-0.4	-4.0	-1.0	4.1
ADY1	-7.5	74.6	-7.6	75.4
AKLE	-1.7	7.6	-2.2	8.04
ANTE	29.8	29.5	1.2	41.9
EKZ1	42.9	-465.3	-12.7	467.4
HAT2	-9.2	-14.9	4.1	17.9
KLS1	25.7	13.7	4.8	29.5
MAR1	-17.3	-59.5	3.1	62.0
MLY1	-64.0	-39.0	0.4	74.9
ONIY	-23.8	-17.7	3.1	29.8

Table 1 shows that the largest deformations occurred at EKZ1 and ADY1 stations. The three-dimensional co-seismic deformation amounts at these stations are 467.42 cm and 75.36 cm, respectively. The co-seismic deformation at MAR1 station, one of the two stations near to the epicentres of the earthquakes, is 62.03 cm. Daily coordinate differences were calculated to clearly see the daily motion of the stations. Since the two near points to the epicentres of the earthquakes are EKZ1 and MAR1, the

coordinate differences of these stations are given in Figure 3 and Figure 4.
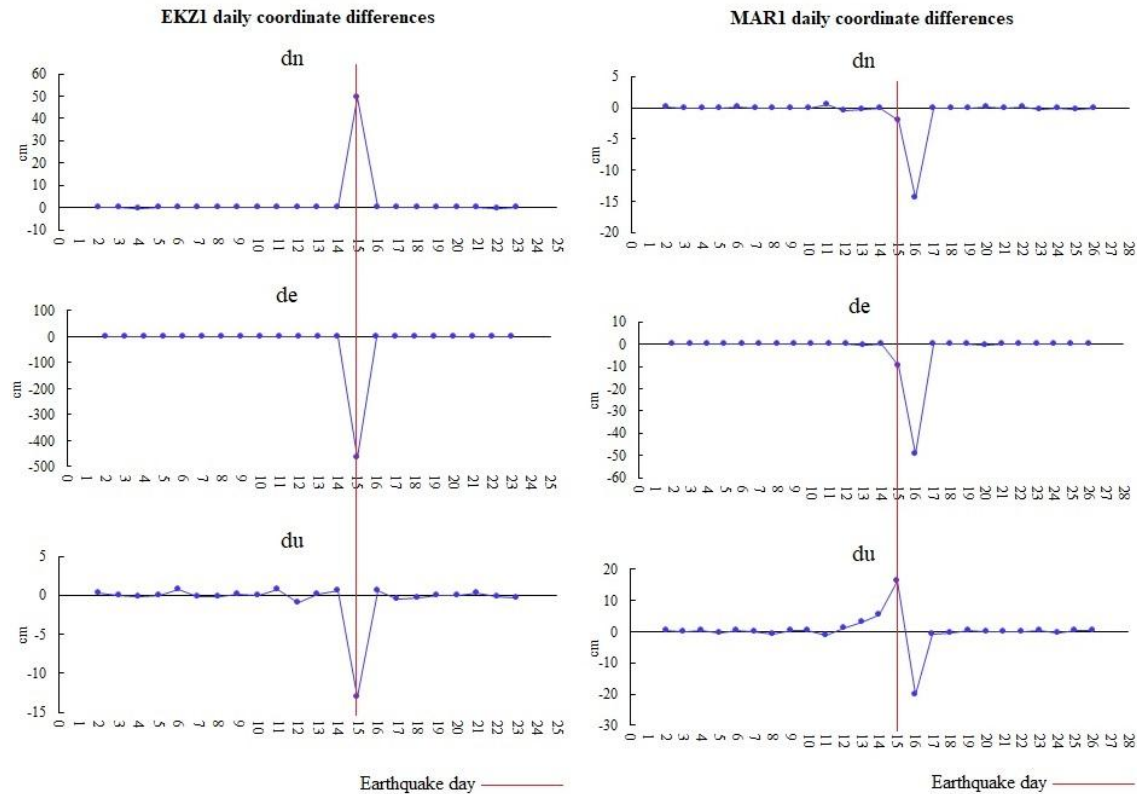
Figure 3. Daily coordinate differences of EKZ1 and MAR1

Figure 3 shows that before the earthquake at EKZ1 station, the coordinate differences in the northern component ranged between 0.1 - 2.4 mm, in the east component between 0.1 - 1.6 mm, and in the up component between 0.4 - 9.6 mm. On the day of the earthquake, a position change of 4.64 meters in the west direction, 49.29 cm in the northward and -13.04 cm in the upward occurred at EKZ1 station, and the positional change decreased and almost approached zero in the days following the earthquake. Similarly, at MAR1 station, while there were mm-level coordinate differences in the days before the earthquake, because of the earthquake, displacement of -49.54 cm in the westward and -14.35 cm in the northward occurred. In the upward direction, the height increased 5.55 cm the day before the earthquake, and with the effect of the earthquake, the station first rose 16.2 cm, and then a 20.14 cm subsidence occurred at the station. There is a possibility that this upward movement, which started two days before the earthquake, can be an earthquake precursor. Because an unusual 15 cm height change occurred at the MAR1 station on the previous day of earthquakes. It is seen that the movement at this station became stable in the following days of earthquake sequence. In order to clearly see the change of the station coordinates, the GPS coordinate time series of these two stations are presented in Figure 4.
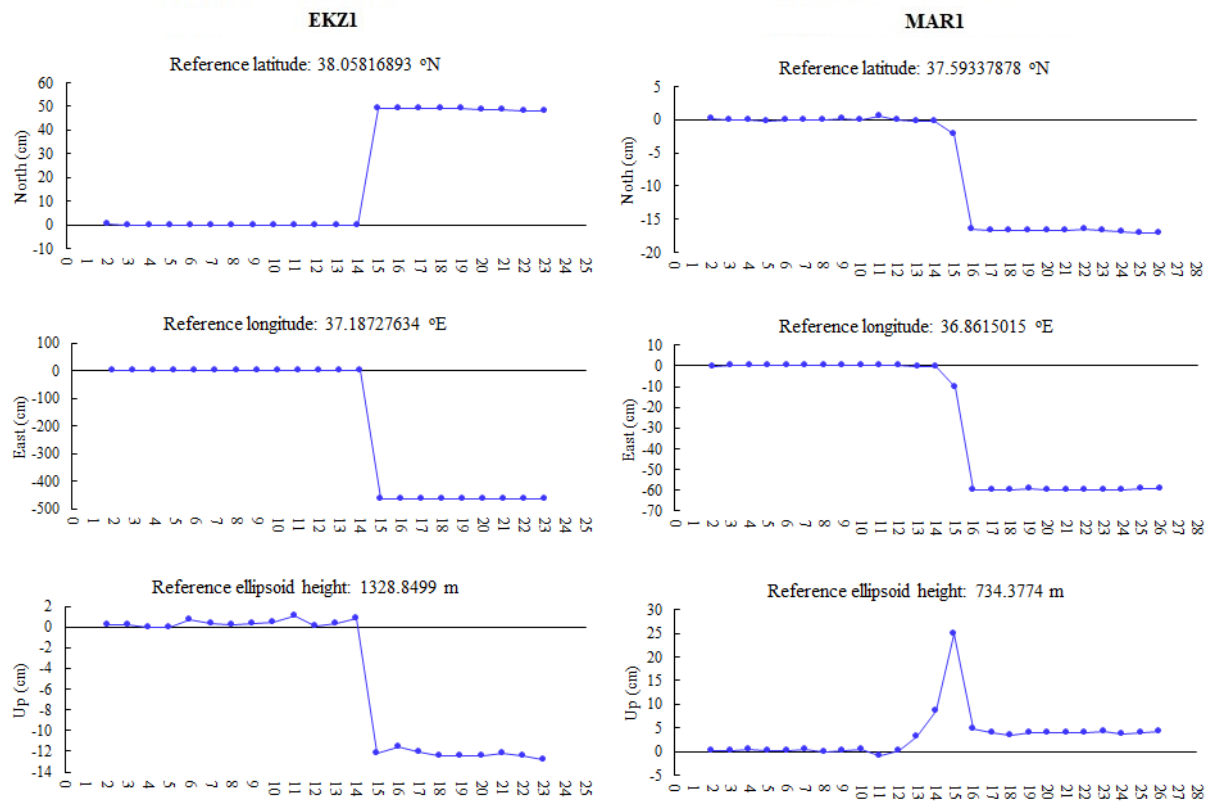
Figure 4. GPS coordinate time series for EKZ1 and MAR1 stations during monitoring

According to Figure 4, while the daily changes in coordinates at EKZ1 station before the earthquake were around 1-2 mm, with the effect of the earthquake, the coordinates of this station changed by 49.22 cm in the north, 464.19 cm in the west, and 12.2 cm in the upward direction. While the coordinates of the MAR1 station changed by 1-2 mm before the earthquake, they changed by 16.55 cm in the northward, 59.7 cm in the westward and 3.5 cm in the upward direction because of the earthquake. Following these pulses, coordinate changes decreased to mm levels after the earthquake in both stations. The height of MAR1 station increased 15 cm on the previous day of the earthquakes. These changes show that the East Anatolian fault, where the stations are located, has slipped approximately 4 meters towards the west. After this stage, two-epoch deformation analyses were carried out for each CORS-Tr station with the IWST method using an in-house software, and the absolute deformations at the stations were determined by performing the final S-transformation. A geodetic network was established to perform deformation analyses. The points of this geodetic network are shown in Figure 5. While designing the deformation network, fourteen IGS stations were considered as reference points and one of CORS-Tr stations in the earthquake impact area were considered as object point. One geodetic network was designed to reveal the deformation at each object point. Thus, since there are ten object points in total, analyses were performed using ten different deformation networks. The analysis results are presented in Table 2, Table 3, and Figure 6.
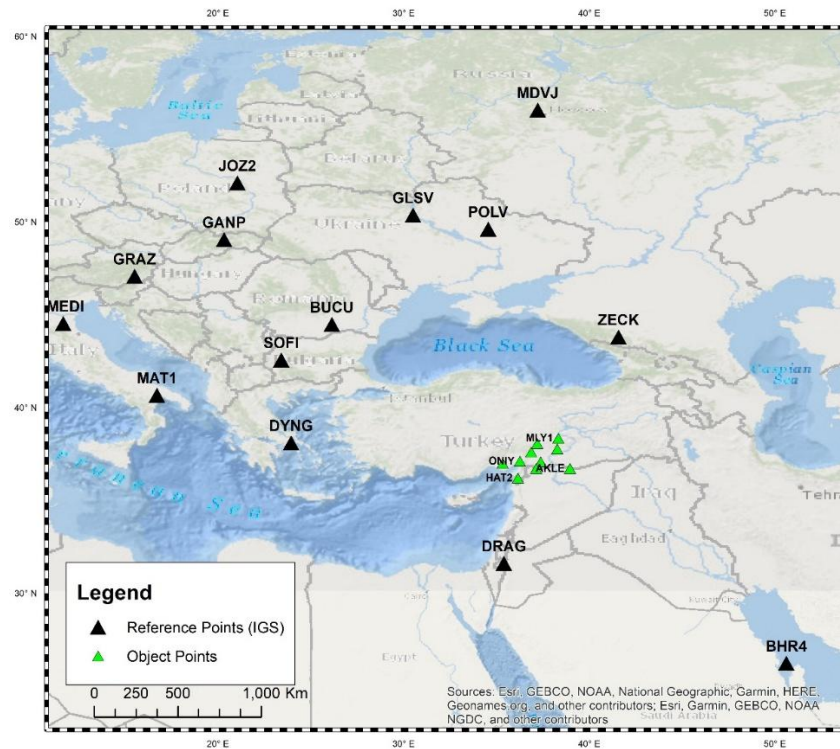
Figure 5. GPS stations of deformation network

Table 2. Deformation analysis results for first four CORS-Tr stations

Station	Disp. Vector (cm)	Test Value	Status	Station	Disp. Vector (cm)	Test Value	Status
BHR4	0.4	6.58	unstable	BHR4	0.3	5.80	unstable
BUCU	0.2	1.65	stable	BOR1	0.2	3.82	unstable
DRAG	0.7	8.44	unstable	BUCU	0.2	3.32	unstable
DYNG	0.9	17.96	unstable	DRAG	0.6	8.10	unstable
GANP	0.2	1.80	stable	DYNG	0.8	18.49	unstable
GLSV	0.1	2.71	unstable	GANP	0.2	1.19	stable
GRAZ	0.2	1.60	stable	GLSV	0.2	10.28	unstable
JOZ2	0.1	2.51	stable	GRAZ	0.3	2.43	stable
KLS1	29.9	41086.58	unstable	JOZ2	0.1	0.24	stable
MAT1	0.5	12.28	unstable	**MAR1**	62.5	726126.73	unstable
MDVJ	0.2	4.99	unstable	MAT1	0.4	9.93	unstable
MEDI	0.1	3.30	unstable	MDVJ	0.2	3.44	unstable
POLV	0.2	1.00	stable	POLV	0.2	0.96	stable
SOFI	1.3	33.93	unstable	SOFI	1.2	28.09	unstable
ZECK	0.7	33.67	unstable	ZECK	0.7	28.14	unstable

| Station	Disp. Vector (cm)	Test Value	Status	Station	Disp. Vector (cm)	Test Value	Status
BHR4	0.3	5.24	unstable	BHR4	0.2	2.59	stable
BUCU	0.3	3.48	unstable	BUCU	0.2	6.10	unstable
DRAG	0.8	18.32	unstable	DRAG	0.1	1.20	stable
DYNG	1.0	18.25	unstable	DYNG	0.6	33.58	unstable
GANP	0.1	0.71	stable	GANP	0.5	5.76	unstable
GLSV	0.2	5.22	unstable	GLSV	0.1	0.20	stable
GRAZ	0.1	0.12	stable	GRAZ	0.2	8.98	unstable
JOZ2	0.1	0.50	stable	JOZ2	0.6	5.44	unstable
MAT1	0.5	4.84	unstable	MAT1	0.0	0.26	stable
MDVJ	0.3	6.29	unstable	MDVJ	0.3	8.40	unstable
MEDI	0.2	1.53	stable	MEDI	0.3	3.41	unstable
ONIY	30.0	117729.31	unstable	**MLY1**	76.1	737259.70	unstable
POLV	0.1	0.77	stable	POLV	0.1	1.66	stable
SOFI	1.3	43.59	unstable	SOFI	1.3	25.33	unstable
ZECK	0.8	47.04	unstable	ZECK	0.7	30.15	unstable

**Table 3.** Deformation analysis results for the second six CORS-Tr stations

Station	Disp. Vector (cm)	Test Value	Status	Station	Disp. Vector (cm)	Test Value	Status	Station	Disp. Vector (cm)	Test Value	Status
ADN2	4.2	2855.86	unstable	**ADY1**	74.7	749076.90	unstable	**AKLE**	8.9	5456.55	unstable
BHR4	0.4	8.97	unstable	BHR4	0.3	4.44	unstable	BHR4	0.4	8.47	unstable
BUCU	0.3	3.07	unstable	BUCU	0.1	2.00	stable	BUCU	0.1	1.83	stable
DRAG	0.7	15.27	unstable	DRAG	0.2	0.90	stable	DRAG	0.3	7.26	unstable
DYNG	1.1	19.11	unstable	DYNG	0.4	5.07	unstable	DYNG	0.7	9.55	unstable
GANP	0.1	0.57	stable	GANP	1.3	21.60	unstable	GANP	1.0	22.69	unstable
GLSV	0.2	4.93	unstable	GLSV	0.5	10.76	unstable	GLSV	0.3	8.35	unstable
GRAZ	0.0	0.12	stable	GRAZ	0.2	4.61	unstable	GRAZ	0.1	3.24	unstable
JOZ2	0.1	1.33	stable	JOZ2	0.5	16.40	unstable	JOZ2	0.3	6.63	unstable
MAT1	0.5	6.93	unstable	MAT1	0.3	8.62	unstable	MAT1	0.1	2.43	stable
MDVJ	0.3	5.36	unstable	MDVJ	0.5	8.29	unstable	MDVJ	0.6	15.36	unstable
MEDI	0.3	5.66	unstable	MEDI	0.1	0.99	stable	MEDI	0.1	0.93	stable
POLV	0.1	0.55	stable	POLV	0.1	1.69	stable	POLV	0.2	1.38	stable
SOFI	1.4	43.40	unstable	SOFI	1.2	25.78	unstable	SOFI	1.4	26.28	unstable
ZECK	0.8	38.07	unstable	ZECK	1.2	56.02	unstable	ZECK	0.8	44.14	unstable

Station	Disp. Vector (cm)	Test Value	Status	Station	Disp. Vector (cm)	Test Value	Status	Station	Disp. Vector (cm)	Test Value	Status
ANTE	42.3	146683.13	unstable	BHR4	0.4	6.96	unstable	BHR4	0.5	13.43	unstable
BHR4	0.5	14.06	unstable	BUCU	0.2	2.07	stable	BUCU	0.2	2.63	unstable
BUCU	0.3	4.68	unstable	DRAG	0.2	4.54	unstable	DRAG	0.2	0.90	stable
DRAG	1.0	33.29	unstable	DYNG	0.4	12.59	unstable	DYNG	0.5	19.04	unstable
DYNG	0.9	17.13	unstable	**EKZ1**	467.5	41158454.66	unstable	GANP	1.0	20.60	unstable
GANP	0.1	2.12	stable	GANP	0.8	27.77	unstable	GLSV	0.1	0.42	stable
GLSV	0.1	3.49	unstable	GLSV	0.3	2.71	unstable	GRAZ	0.1	4.07	unstable
GRAZ	0.1	0.46	stable	GRAZ	0.2	5.78	unstable	**HAT2**	17.7	46830.74	unstable
JOZ2	0.1	0.47	stable	JOZ2	0.3	5.30	unstable	JOZ2	0.2	4.95	unstable
MAT1	0.5	15.18	unstable	MAT1	0.1	2.07	stable	MAT1	0.0	0.56	stable
MDVJ	0.1	3.03	unstable	MDVJ	0.4	9.06	unstable	MDVJ	0.3	7.66	unstable
MEDI	0.1	1.97	stable	MEDI	0.2	2.45	stable	MEDI	0.1	3.37	unstable
POLV	0.3	1.59	stable	POLV	0.2	1.17	stable	POLV	0.2	3.80	unstable
SOFI	1.3	26.77	unstable	SOFI	1.2	29.85	unstable	SOFI	1.3	40.21	unstable
ZECK	0.8	48.22	unstable	ZECK	0.8	48.46	unstable	ZECK	0.8	37.70	unstable

Table 2 and Table 3 show deformation analysis results after the final S-transformation. Ten different deformation analyses were carried out for each CORS-Tr station. The critical value in the analysis is 2.605. Significant point movements were determined by comparing the test value with 2.605 and shown in the status column of Table 2. According to the results of the IWST, four or five IGS points remained stable. Significant displacements were observed at the other IGS points even if they were approximately 1500 km away from the region. Although the selected IGS reference stations are located outside the earthquake-affected region, some of them were classified as "unstable" in the deformation analysis. This may be due to several factors, such as long-distance baseline geometry, slight tectonic activity in the surrounding areas, or inconsistencies in daily coordinate solutions. In some cases, if the statistical compatibility of measurements between two epochs is not satisfied, it may result in the station being falsely flagged as unstable. To mitigate this, inconsistent measurement and variance homogeneity tests were performed between the two adjustment epochs (Equation 3), and the final S-transformation was applied based only on the most stable IGS stations. Nonetheless, the observed instability in certain distant IGS stations highlights the importance of rigorous station selection and testing in global network-based deformation analyses. When we look at the displacement vectors calculated as a result of the S-transformation, it is seen that they are compatible with the co-seismic deformations which were given in Table 1. Most of the displacement vectors at the reference IGS points are smaller than 5 mm. As a result of IWST, the stable IGS points were taken as datum and the absolute deformations at the CORS-tr stations were determined. These displacement vectors representing the absolute deformations of the CORS-Tr stations are presented in Figure 6.
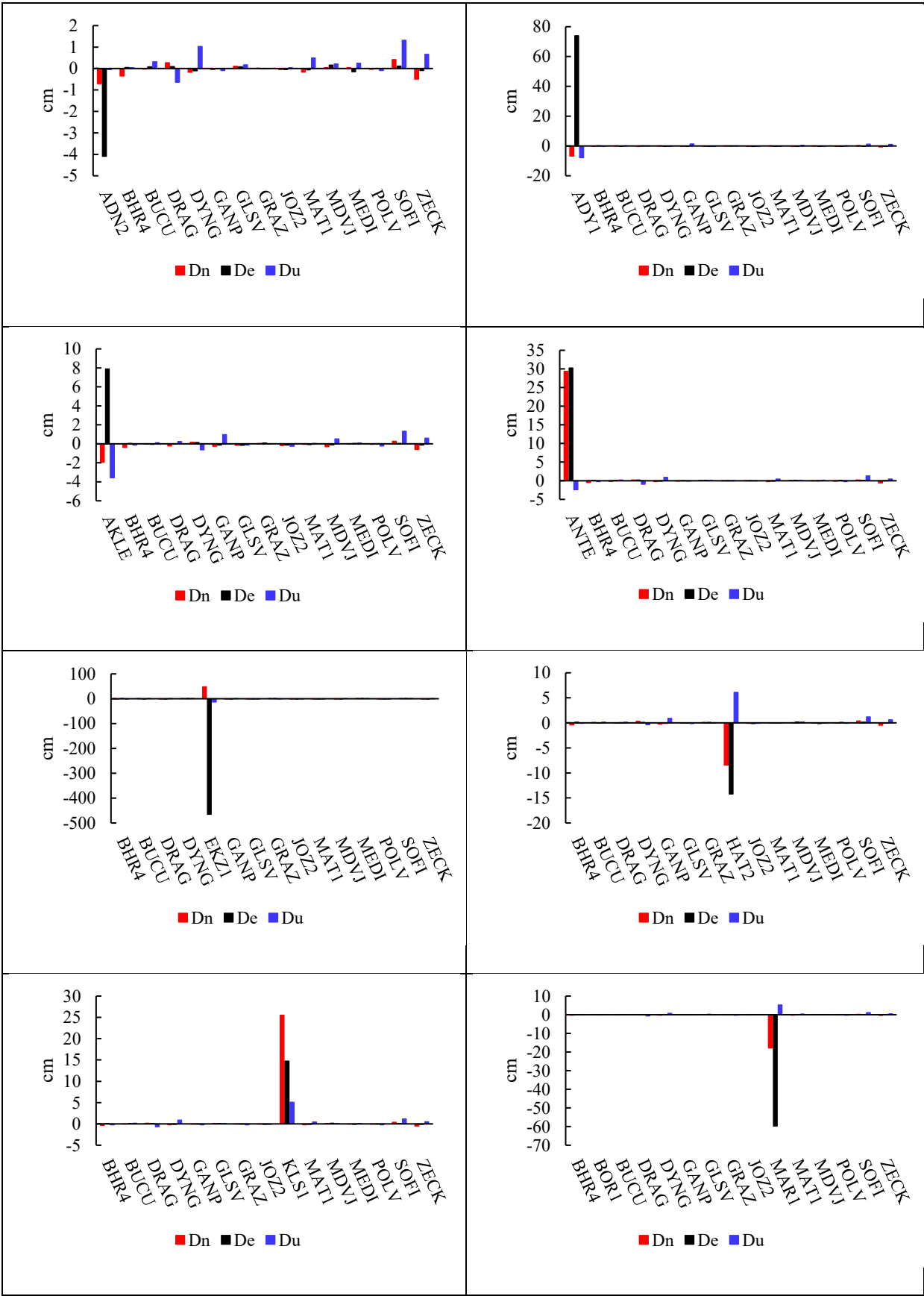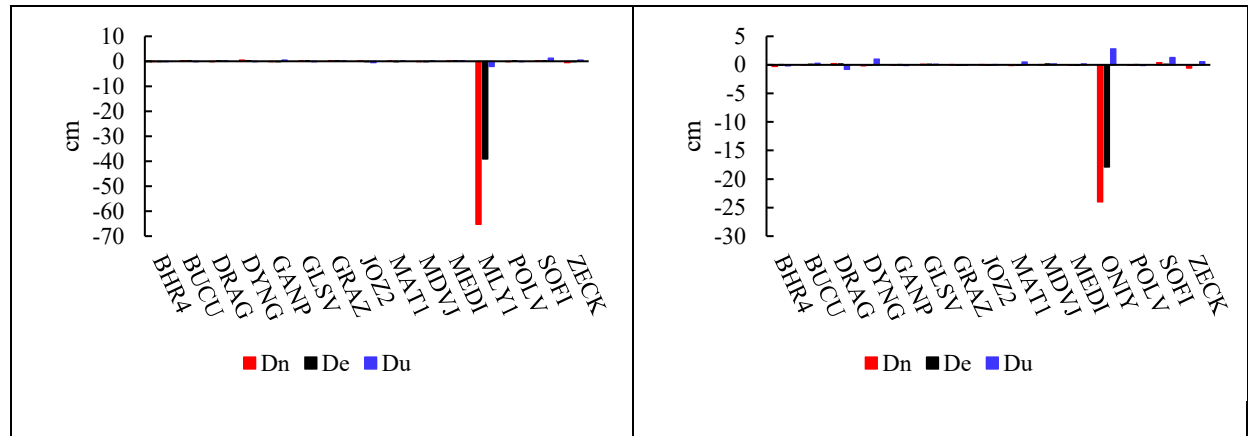
Figure 6. Absolute deformations in the direction of topocentric coordinate axes

In Figure 6, each graph shows the absolute deformations for one CORS-Tr station in the earthquake zone. Since the IWST and final S-transformation are used in deformation analyses, all stations of the geodetic deformation network are also seen in the graphics. The graphs show that the largest absolute deformation occurred at the EKZ1 station with 4.68m, that was the closest station to the epicentre of the aftershock (Mw 7.6). The absolute deformation at station MAR1, which is the second near station to the epicentre of the aftershock, is 62.5 cm. This value is 17.6 cm at the HAT2 station in Hatay, where great destruction occurred due to the earthquake. Absolute deformations at ADN2 in Adana, ADY1 in Adıyaman, AKLE in Şanlıurfa, ANTE in Gaziantep, KLS1 in Kilis, MLY1 in Malatya and ONIY in Osmaniye are 4.2 cm, 74.7 cm, 8.9 cm, 42.3 cm, 29.9 cm, 76.1 cm, and 30.1 cm, respectively.

4. CONCLUSIONS

Earthquake is a phenomenon that effects human life, especially earthquake prone regions such as Türkiye. This phenomenon leads to deformations on the earth's crust. Crustal deformations could be monitored using geodetic GPS networks. Tectonic plates that cause earthquakes also need to be monitored with GPS networks today. The Kahramanmaraş earthquake sequence that occurred on 6 February 2023, once again revealed this necessity, and showed that the positions of CORS stations should be constantly monitored.

In this study, the movements of CORS-Tr stations affected by the Kahramanmaraş earthquakes in Türkiye were investigated in detail. Ten stations were selected from the provinces where the earthquake was felt, and their 28-day data covering the pre- and post-earthquake periods were processed with AUSPOS online GPS processing software. After the processing, the movements at the stations were examined in detail through time series, coordinate differences and deformation analyses using the geodetic network method.

For this purpose, the co-seismic deformations first determined at the stations varied between 0.4 cm and 64 cm in the northern component, between 3.8 cm and 465.3 cm in the eastern component, and between 0.2 cm and 12.7 cm for upward component. The largest co-seismic deformations occurred at EKZ1 in Kahramanmaraş. These results are consistent with [12] and [13]. This was followed by ADY1 stations in Adıyaman, MLY1 in Malatya, MAR1 in Kahramanmaraş, ANTE in Gaziantep, ONIY in Osmaniye, KLS1 in Kilis, HAT2 in Hatay, AKLE in Şanlıurfa, and ADN2 in Adana, respectively.

When looking at the daily coordinate differences at the stations during the monitoring period, the obtained results showed that there were unusual horizontal and vertical movements a day or two days before the earthquake. It was observed that the increasing height and horizontal slips that occurred one day ago, especially at the MAR1 station, were outside the usual values. When the time series of the two stations are examined, it is seen that very large slips occur because of the earthquake. It has been determined that the Anatolian plate slipped approximately 4 meters westward because of these pulses.

For each station, the absolute deformations caused by the earthquake were revealed through

deformation analyses performed using GPS data processing results of one day before and after the earthquake. Final S-transformation-based absolute deformations and average coordinate-based co-seismic deformations are very close to each other. According to the graphics of the deformation analysis results, significant movements were observed at all CORS-Tr stations examined and the largest absolute deformation occurred at EKZ1 station with 4.68 m. It was also observed that 4 or 5 reference IGS points furthest from the earthquake zone could remain stable. These findings have shown that the IWST and final S-transformation are reliable methods that should be used in determining absolute deformations. It has also been revealed that the data processing results (coordinates, root mean square errors and covariance matrices) obtained from the AUSPOS online GPS processing service can be used in geodetic deformation analysis.

Future research could focus on integrating high-rate GPS or InSAR data with AUSPOS-derived results to better detect short-term pre-seismic anomalies, and to develop automated early warning frameworks for seismic risk assessment.

Declaration of Ethical Standards

The author declares that the study complies with all applicable laws and regulations and meets ethical standards.

Declaration of Competing Interest

The author declares that he has no known competing financial interests or personal relationships that could have appeared to influence the work reported in this paper.

Funding / Acknowledgements

The author declares that no funding was used in the study.

Data Availability

The dataset used and/or analysed during the current study are available from corresponding author on reasonable request.

5. REFERENCES

[1]   S. Jin, G. Occhipinti, and R. Jin, "GNSS ionospheric seismology: recent observation evidences and characteristics", *Earth Sci. Rev.* vol. 147, pp. 54–64, 2015, doi: 10.1016/j.earscirev.2015.05.003.

[2]   S. Uplines, and K. Boyarchuk, *Ionospheric Precursors of Earthquakes.* Springer Science & Business Media, 2004.

[3]   V. Atasoy, and E. Ozturk, "Geodetic Deformation Measurements and Interpretation of Results", *TMMOB Journal of Surveying Engineering*, (In Turkish), pp. 50-51, 1984.

[4]   B. Bilgen and C. İnal, "Investigation of Vertical Deformations with GNSS Technique", *Afyon Kocatepe University Journal of Science and Engineering*, vol. 22, no. 3, pp. 615–625, 2022, doi: 10.35414/akufemubid.1066483.

[5]   B. Bilgen, C. İnal, and S. Bülbül, "Point Positioning Performanceo Trimble-RTX in Different Satellite Combinations", *KONJES*, vol. 10, no. 4, pp. 941–949, 2022, doi: 10.36306/konjes.1165922.

[6]   H. Ozener, E. Arpat, S. Ergintav, A. Dogru, R. Cakmak, B. Turgut, and U. Dogan, "Kinematics of the eastern part of the North Anatolian Fault Zone", *Journal of geodynamics*, vol. 49, no. 3-4, pp. 141-150, 2010, doi: 10.1016/j.jog.2010.01.003.

[7]   A. Gualandi, E. Serpelloni, and M.E. Belardinelli, "Space–time evolution of crustal deformation related to the Mw 6.3, 2009 L'Aquila earthquake (central Italy) from principal component analysis inversion of GPS position time-series", *Geophys. J. Int.,* vol. 197, no. 1, pp. 174–191, 2014, doi:

10.1093/gji/ggt522.

[8]   R.K. Dumka, S. Chopra, S. Prajapati, "GPS derived crustal deformation analysis of Kachchh, zone of 2001(M7.7) earthquake, Western India", *Quaternary International,* vol. 507, pp. 295-301, 2019, doi: 10.1016/j.quaint.2019.01.032.

[9]   A.Z. Sha'ameri, W.A. Wan Aris, S. Sadiah, T.A. Musa, "Reliability of Seismic Signal Analysis for Earthquake Epicenter Location Estimation Using 1 Hz GPS Kinematic Solution", *Measurement,* vol. 182, art no. 109669, 2021, doi: 10.1016/j.measurement.2021.109669.

[10] C.O. Yigit, A. El-Mowafy, A.A. Dindar, M. Bezcioglu, and I. Tiryakioglu, "Investigating Performance of High-Rate GNSS-PPP and PPP-AR for Structural Health Monitoring: Dynamic Tests on Shake Table", *Journal of Surveying Engineering,* vol. 147, no. 1, pp. 1-14, 2021, doi: 10.1061/(ASCE)SU.1943-5428.0000343.

[11] M. Bezcioglu, C.O. Yigit, B. Karadeniz, A.A. Dindar, A, El-Mowafy, and O. Avci, "Evaluation of real-time variometric approach and real-time precise point positioning in monitoring dynamic displacement based on high-rate (20 Hz) GPS Observations" *GPS Solutions,* vol. 27, art no. 43, 2023, doi: 10.1007/s10291-022-01381-6.

[12] S. Bulbul, T. Gundogan, C. Inal, F. Basciftci, and O. Yildirim, "Monitoring deformations caused by Pazarcık (Mw = 7.7) and Ekinözü (Mw = 7.6) earthquakes in Kahramanmaraş on 6 February 2023 with GNSS" *Eur. Phys. J. Plus,* vol. 138, art no. 1110, 2023, doi: 10.1140/epjp/s13360-023-04759-8.

[13] A. Ozkan, H.I. Solak, I. Tiryakioglu, M.D. Senturk, B. Aktuğ, C. Gezgin, F. Poyraz, H. Duman, F. Masson, G. Uslular, C.O. Yigit, H. Yavasoglu, "Characterization of the co-seismic pattern and slip distribution of the February 06, 2023, Kahramanmaraş (Türkiye) earthquakes (Mw 7.7 and Mw 7.6) via dense GNSS network", *Tectonophysics,* vol. 866, art no. 230041, 2023, doi: 10.1016/j.tecto.2023.230041.

[14] W. Li, L. Zhao, K. Tan, X. Lu, C. Zhang, C. Li, and S. Han, "Coseismic deformation and fault slip distribution of the 2023 Mw 7.8 and Mw 7.6 earthquakes in Türkiye", *Earthquake Science,* vol. 37, pp. 263-276, 2024, doi: 10.1016/j.eqs.2024.03.006.

[15] T. Taymaz, A. Ganas, S. Yolsal-Çevikbilen, F. Vera, T. Eken, C. Erman, D. Keleş, V. Kapetanidis, S. Valkaniotis, I. Karasante, V. Tsironi, P. Gaebler, D. Melgar, and T. Öcalan, "Source Mechanism and Rupture Process of the 24 January 2020 Mw 6.7 Doğanyol–Sivrice Earthquake obtained from Seismological Waveform Analysis and Space Geodetic Observations on the East Anatolian Fault Zone (Turkey)", *Tectonophysics,* vol. 804, art no. 228745, 2021, doi: 10.1016/j.tecto.2021.228745.

[16] C. Bayik, G. Gurbuz, S. Abdikan, K.S. Gormus, and S.H. Kutoglu, "Investigation of Source Parameters of the 2020 Elazig-Sivrice Earthquake (Mw 6.8) in the East Anatolian Fault Zone", *Pure Appl. Geophys.,* vol. 179, pp. 587–598, 2022, doi: 10.1007/s00024-022-02944-x.

[17] O. Gunaydin, Y. Inceyol, H. Cetin, M. Ulukavak, "Fault displacement analysis using a multidisciplinary approach on the Gerede Segment of the North Anatolian Fault Zone", *Soil Dynamics and Earthquake Engineering,* vol. 164, art no. 107519, 2023, doi: 10.1016/j.soildyn.2022.107519.

[18] T. Kobayashi, H. Munekane, M. Kuwahara, and H. Furui, "Insights on the 2023 Kahramanmaraş Earthquake, Turkey, from InSAR: fault locations, rupture styles and induced deformation", *Geophysical Journal International,* vol. 236, pp. 1068-1088, 2024, doi: 10.1093/gji/ggad464.

[19] A. Gualandi, H. Perfettini, M. Radiguet, N. Cotte, and V. Kostoglodov, "GPS deformation related to the Mw 7.3, 2014, Papanoa earthquake (Mexico) reveals the aseismic behavior of the Guerrero seismic gap", *Geophys. Res. Lett.,* vol. 44, pp. 6039–6047, 2017, doi:10.1002/2017GL072913.

[20] Y. Wu, Z. Jiang, J. Zhao, X. Liu, W. Wei, Q. Liu, Q. Li, Z. Zou, and Z. Zhang, "Crustal deformation before the 2008 Wenchuan MS8.0 earthquake studied using GPS data", *Journal of Geodynamics,* vol. 85, pp. 11-23, 2015, doi: 10.1016/j.jog.2014.12.002

[21] E. Klein, C. Vigny, L. Fleitout, R. Grandin, R. Jolivet, E. Rivera, M. Métois, "A comprehensive analysis of the Illapel 2015 Mw8.3 earthquake from GPS and InSAR data", *Earth and Planetary Science Letters,* vol. 469, pp. 123-134, 2017, doi: 10.1016/j.epsl.2017.04.010.

[22]   L. Wang, H. Gao, G. Feng, W. Xu, "Source parameters and triggering links of the earthquake sequence in central Italy from 2009 to 2016 analyzed with GPS and InSAR data", *Tectonophysics,* vol. 744, pp. 285-295, 2018, doi: 10.1016/j.tecto.2018.07.013.

[23]   T. Taymaz, H. Eyidogan, and J. Jackson, "Source parameters of large earthquakes in the East Anatolian Fault Zone (Turkey)", *Geophysical Journal Int.,* vol. 106, pp. 537-550, 1991, doi: 10.1111/j.1365-246X.1991.tb06328.x.

[24]   C.R. Allen, "Active faulting in northern Turkey", Contr.1577. Division of Geology Sciences, California Institute of Technology, 1969.

[25]   H. Cetin, H. Güneyli, L. Mayer, "Paleoseismology of the Palu–Lake Hazar segment of the East Anatolian Fault Zone, Turkey", *Tectonophysics,* vol. 374, no. 3-4, pp. 163-197, 2003, doi: 10.1016/j.tecto.2003.08.003.

[26]   F. Bulut, M. Bohnhoff, T. Eken, C. Janssen, T. Kılıç, G. Dresen, "The East Anatolian Fault Zone: Seismotectonic setting and spatiotemporal characteristics of seismicity based on precise earthquake locations", *Journal of Geophysical Research,* vol. 117, no. B7, pp. 1-16, 2012, doi: 10.1029/2011JB008966.

[27]   NN. Ambraseys, and J.A. Jackson, "Faulting associated with historical and recent earthquakes in the Eastern Mediterranean region", *Geophysical Journal International,* vol. 133, no. 2, pp. 390-406, 1998, doi: 10.1046/j.1365-246X.1998.00508.x.

[28]   AFAD, "Preliminary Assessment Report on 06 February 2023 Pazarcık (Kahramanmaraş) Mw 7.7, Elbistan (Kahramanmaraş) Mw 7.6 Earthquakes", Earthquake Department, pp. 1-12, 2023.

[29]   D. Ö. Demir and Ö. Güneş, "29 Temmuz 2021 Mw=8.2 Chignik, Alaska Peninsula depremi deformasyonlarının bağıl konum belirleme servis sonuçları ile incelenmesi", *NÖHÜ Müh. Bilim. Derg.,* vol. 13, no. 2, pp. 575–581, 2024, doi: 10.28948/ngumuh.1387411.

[30]   M. Hanif and S. Tongleamnak, "Quantifying crustal deformation caused by the Cianjur tectonic earthquakes magnitude 5.6 through DInSAR and GNSS technology", *Bulletin of Earth Sciences of Thailand,* vol. 16, no. 1, pp. 60-71, 2024. https://ph01.tci-thaijo.org/index.php/bestjournal/article/view/256321

[31]   B. Hoffman-Wellenhof, H. Lichtenegger, and E. Wasle, *GNSS - Global Navigation Satellite Systems,* Austria, Springer, 2008.

[32]   Y.Q. Chen, A. Chrzanowski, J.M. Secord, "A strategy for the analysis of the stability of reference points in deformation surveys" *Cism J ACSGS,* vol. 44, no. 2, pp. 141–149, 1990, doi: 10.1139/geomat-1990-0016.

[33]   E. Gokalp, L. Tasci, "Deformation monitoring by GPS at embankment dams and deformation analysis" *Surv Rev,* vol. 41, no. 311, pp. 86–102, 2009, doi: 10.1179/003962608X390021.

[34]   B. Konakoglu, and E. Gokalp, "Deformation Measurements and Analysis with Robust Methods A Case Study Deriner Dam", *Turkish Journal of Science and Technology,* vol. 13, no. 1, pp. 99–103, 2018.

[35]   S. Doganalp, B. Turgut, and C. Inal, "Deformation Analyses by Kalman Filtering and S Transformation Techniques for Height Networks", (in Turkish), In Proc. 2nd Symposium of Engineering Surveys, 23-25 Nov. 2005, İstanbul.

[36]   C.O. Yigit, C. Inal, "An Improved Programme for Deformation Analysis of Vertical Networks", In Proc. XXIII FIG Congress, Munich, Germany, 2006.

[37]   G. Even-Tzur, "Extended S-transformation as a tool for deformation analysis", *Survey Review,* vol. 44, no. 327, pp. 315-318, 2012, doi: 10.1179/1752270612Y.0000000005.

[38]   H. Velsink, "On the deformation analysis of point fields", *Journal of Geodesy,* vol. 89, pp. 1071-1087, 2015, doi: 10.1007/s00190-015-0835-z.

[39]   C. Aydin, "Effects of Displaced Reference Points on Deformation Analysis", *Journal of Surveying Engineering,* vol. 143, no. 3, 2017, doi: 10.1061/(ASCE)SU.1943-5428.0000216.